Physicochem. Probl. Miner. Process., 59(1), 2023, 161510

http://www.journalssystem.com/ppmp

Physicochemical Problems of Mineral Processing

ISSN 1643-1049

Role of ammonium phosphate in improving the physical characteristics of malachite sulfidation flotation

Ayman M. Ibrahim [1,2], Xiaodong Jia [1], Jinpeng Cai [1], Chao Su [1], Xingcai Yu [1], Qifang Zheng[1], Rong Peng [1], Peilun Shen [1], Dianwen Liu [1]

[1] Faculty of Land Resources Engineering, Kunming University of Science and Technology, Kunming, 650093, China

[2] Department of Mining Engineering, University of Nyala, Sudan

Corresponding authors: peilunshen@kust.edu.cn (Peilun Shen), dianwenliu@kust.edu.cn (Dianwen Liu)

Abstract: In this study, ammonium phosphate ($(NH_4)_3PO_4$) was employed to realize improvement by modifying the physical characteristics of the malachite surface, ensuring sustainable flotation throughout the flotation operations, and enhancing the flotation process to be more stable. Furthermore, various techniques, including X−ray photoelectron spectroscopy, were intensely used to investigate the configuration and physico-chemical surface characteristics through micro-flotation experiments, contact angle and zeta potential measurements, and XRD, ToF−SIMS, EPMA, and FTIR spectrum analyses. The FTIR findings showed that new characteristic peaks of −C(=S)−N.H. groups formed and adsorbed on the surfaces of malachite at 1636 cm^{-1}. The $-CH_2$ groups throughout the flotation process, further promoted the attachment of the CH_3 ligand to the Cu^{2+} ion, and the XPS analysis confirmed this. Consequently, it can be concluded that $(NH_4)_3PO_4$ played a substantial part in the improved recovery rate, as demonstrated and confirmed by the methods carried out in this study. Thus, it was used to modify the physical properties surface before adding Na_2S to efficiently enhance malachite floatability and reduce the loss rate of malachite. Regarding the alterations in the physical characteristics which occurred to the malachite surface, and as a consequence of increasing the recovery results of flotation, the malachite sample treated initially with $(NH_4)_3PO_4$ exhibited micro flotation results with a considerably greater flotation recovery than malachite treated initially with only Na_2S ions.

Keywords: malachite sulfidation, sample preparation, ammonium phosphate, sodium sulfide, floatability, physical characteristics

1. Introduction

Copper is currently one of the most widely utilized nonferrous metals in chemical engineering, construction, and military applications. Presently, copper is produced mainly through the refining of copper sulfide ores. Moreover, it is common knowledge that mineable mineral resources are developed. The grade will inevitably decrease as a natural progression of the process (Hu et al., 2020; Cai et al., 2021).

Malachite is a common copper oxide mineral that primarily consists of $CuCO_3$ and $Cu(OH)_2$, which should be sufficiently exploited to ensure the long-term viability of copper resources (Cecile et al., 1981; Li et al., 2020). The available copper sulfide resources are depleting as copper consumption and demand rise (Chen et al., 2014; Sheng et al., 2021). The mineral occurs in the carbonate rock's oxidation zone and skarn-type copper deposits. However, a copper-bearing industrial mineral is essential for producing copper metal (Feng et al., 2018; Liu et al., 2018; Wang et al., 2022). For non-sulfide and mixed non-sulfide besides sulfide copper ores with high carbonate components or low copper content, froth flotation becomes the preferred separation and upgrading technique for copper minerals (Lee et al., 1998; Liu et al., 2018; Belkassa et al., 2021). These minerals include malachite ($CuCO_3.Cu(OH)_2$), azurite ($2CuCO_3.Cu(OH)_2$), chrysocolla ($CuSiO_3.2H_2O$), and cuprite (Cu_2O). Flotation methods can be classified as either direct as well as sulfidation flotation. The last technique is the most commonly used method for industrial-scale enrichment of copper oxide ores (Wang et al., 2020; Han et al., 2021a).

DOI: 10.37190/ppmp/161510

One of the most important steps to recover non-sulfide copper minerals through flotation is surfactant-selectively hydrophobic of the minerals (known as a flotation collector). Adsorption occurs when air (or nitrogen) bubbles attach to hydrophobic mineral particles and transfer them to the pulp/air interfaces (He et al., 2016; Huang et al., 2019). Throughout this process, the mineral particles in an aqueous pulp attach to air bubbles to form particle/bubble aggregates transferred out of the pulp. The sulfurization mechanism involves the ionization of sodium sulphide (Na_2S) HS^- and S^{2-} ions that undergo an absorption process with copper ions on the surface of copper oxide minerals (Chen et al., 2021). Sodium sulfide dosage is the essential factor influencing the sulfidization flotation of copper oxide minerals. Therefore, inadequate extra doses are not promotive to flotation (Han et al., 2021b). Surface improvement has been applied to enhance the sulfidization flotation of copper oxide minerals. However, adding ammonium sulfate ($(NH_4)_3PO_4$)) in the sulfidization flotation of copper-oxide minerals could avoid the depression of excessive Na_2S.

Moreover, it has been reported that the activators such as ethylene diamine phosphate, $(NH_4)_3PO_4$, and ammonium bisulfate enhance the sulfidization of copper oxide mineral surface (Sheng et al., 2021). This reduces the amount of sulfurizing reagent necessary and significantly improves the hydrophobicity of the minerals, which enhances flotation recovery (Feng et al., 2017; Wu et al., 2017). The surface topography variations are inadequately described. As a result, there was little consensus on how organic ligands influence the malachite surface properties after being activated with NH_4^+ groups (Yoshimura et al., 1972; Thakur et al., 1972).

Throughout this research study, micro-flotation experiments, EPMA, contact angle, XPS, FTIR, XRD, and ToF−SIMS analyses were conducted to investigate the possibility of floating by changing and improving the physical characteristics of the malachite surface using various chemical reagents. Moreover, it looks at how the sulfurization process modifies the hydrophobicity, morphology, phase composition, element composition, and state of the malachite surface.

2. Materials and methods

2.1. Materials

The malachite sample used in this study was obtained from Yunnan, China. X−ray fluorescence (XRF) spectroscopy was employed to determine the elemental composition of malachite samples, and the results are listed in Table 1. The main elements and compounds were Cu, Co, Fe, Mn, CaO, MgO, Al_2O_3, and SiO_2. The quantitative analysis indicated that the sample contained 56.14 wt.% Cu. It confirmed the presence of malachite. In addition, malachite samples ($Cu_2CO_3(OH)_2$) were acquired from Yunnan, China, and after that was crushed in the double roll laboratory crusher before being ground in an agate mortar separately. Then, the ground samples were sieved to obtain a −74+37 μm sized sample for the flotation experiments.

Table 1. The XRF analysis results of malachite composition

Elements	Cu	Mn	Fe	SiO_2	Al_2O_3	CaO	MgO	Others
Wt. (%)	56.14	0.400	0.100	2.320	0.560	0.700	0.321	39.459

$(NH_4)_3PO_4$ (Fuyu Fine Chemical Co., Ltd., China) was used to enhance the surface of malachite. $Na_2S.9H_2O$ (Tianjin Guangfu Technology Co., Ltd., China) was used for sulfidization. Sodium butyl xanthate (NaBX, Zhuzhou Flotation Reagents Co., Ltd., China) was used as a collector. HCl and NaOH were used as pH regulators. All reagents were of analytical grade except NaBX for an industrial grade.

2.2. Methods

2.2.1. Sample preparation

The malachite ore (4-5 kg) was crushed first with a hand hummer crushed. Then, nearly 70-80% of the sample was crushed to minus ¼ inch by size, it was thoroughly blended and passed through the sets of sieves several times. Next, the crushed malachite sample was subdivided into two parts, each weighing between 1 and 2 kg. One part was saved for further studies and was ground the other portions of the

malachite sample in a laboratory grinding mill (small scale). Furthermore, the particle size determinations of the ground samples were carried out with wet or dry material sieving. Moreover, the sieves were predominantly agitated to expose all the particles to the sieve openings. Fig. 1 shows the preparation of the malachite ore sample (−74 + 37 μm).

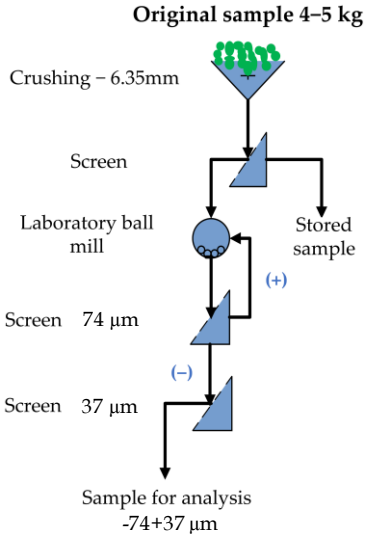

Fig. 1. Preparation of malachite ore sample

2.2.2. Single mineral micro-flotation experiments

The micro-flotation experiments were conducted in an XFGC II flotation apparatus with a cell volume of 40 cm^3, and the impeller speed was maintained at 1200 rpm. In each test, first, a total of 0.5 g of each sample was washed for 5 min with deionized (DI) water in an ultrasonic device. As shown in Fig. 2, regulators were added before applying the collectors for 3 min. Afterward, the sample was placed in the frother and mixed for 1 min. The total time of the flotation process was 4 min. The foam mass was acquired manually. Subsequently, the recovery was estimated by dividing the total dry mass (float product and sink) by the dry weight of the float using Eq. 1:

$$\varepsilon = \frac{m_1}{m_1+m_2} \times 100\% \quad (1)$$

where m_1 and m_2 are the foam and tailing product recoveries, respectively.

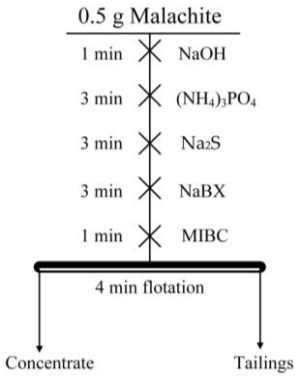

Fig. 2. Flowsheet of single mineral micro-flotation experiments

2.2.3. XRD analysis

XRD analysis was carried out using X'Pert Pro (Malvern Panalytical Ltd., Malvern, Worcestershire, United Kingdom). A tiny portion of the sample weighing 0.2 g was pulverized manually with an agate mortar. Afterward, the XRD patterns were determined at room temperature with CuKα radiation with a wavelength of 1.5406. Patterns of XRD were recorded at 2θ angles between 20° and 85°. Ultimately, Mjd Jade 6.5 software was used to analyze XRD results.

2.2.4. Contact angle measurements

The contact angle measurements were carried out with a JY−82 contact angle analyzer. Malachite samples were processed under various conditions after being polished with 500 grit and 4000 grit Al_2O_3 sandpaper; afterward, the drop shape was taken with a camera. The pictures were then processed by ImageJ 1.46r software (National Institute of Health, Wayne Rasband, USA) and archived. Ultimately, the contact angle measurements were carried out at least twice for each condition.

2.2.5. FTIR analysis

The FTIR analysis was performed using a Nicolet IS50 spectrometer (Thermo Nicolet, USA) to study the modification of reagents interaction on the malachite surface using the wavenumber range of 3100−700 cm^{-1}. Malachite samples were prepared and washed using an ultrasonic device. Afterward, fresh $(NH_4)_3PO_4$ and Na_2S were ready for all experiments. Respectively, malachite particle 2 g was added to a 100 cm^3 volumetric flask, 40 cm^3 of DI water was entered, and HCl and NaOH were used to adjust pH around 9. Finally, all FTIR analysis was done and dried in a vacuum dryer at 100°C.

2.2.6. Zeta potential measurements

A ZetaPlus analyzer (Brookhaven Instruments, USA) was used to measure the zeta potential of the malachite particles in distilled water with varying pH values and initial reagent concentrations. Moreover, the liberation size of malachite samples was prepared for all experiments at about 5 μm and placed in lab glass with electrolyte solution 1×10^{-3} mol/dm^3 KNO_3. Afterward, 0.5 g malachite samples with $(NH_4)_3PO_4$ and Na_2S solutions (if needed) were mixed. Besides, the pH of the solution was adjusted. The suspensions of zeta potential were stirred and separately detected five times after every 4 min of agitation. Ultimately, the average malachite zeta potential was calculated using the average values of three measurements.

2.2.7. XPS analysis

X-ray Photoelectron Spectroscopy (XPS) is a photoemission experiment for spectroscopic analysis. The widespread availability of instruments with enhanced resolution, automatic data acquisition, and monochromatic primary radiation has made deconvolution procedures simple and quick (Sarojini and Vijayalakshmi., 2022). XPS is a surface analysis technique that can investigate solid surfaces' elemental composition and chemical valence.

X-ray Photoelectron Spectroscopy analysis was carried out using a PHI5000 Versa Probe II (PHI5000, ULVAC−PHI Inc., Chigasaki, Kanagawa, Japan) to analyze the surface species of malachite produced by flotation under various reaction conditions and the XPS samples were prepared by adding 0.5 g malachite sample in 40 cm^3 lab glass with DI water. Moreover, malachite samples were washed, filtered, dried, and placed in a silica gel desiccator for storage. Wherever the spectrum was calibrated with the C1s peak at 284.8 eV as a standard, then 30 KeV Al Kα X−ray (hv = 1486.6 eV) was used. Consequently, high spectra resolution of the C1s, O1s, S 2p, and Cu 2p3/2 core level zones were acquired at 20 eV pass energy with 0.2 eV steps. Furthermore, the XPS results for the malachite sample were collected and processed by MultiPak 6.5 software & origin 2021 software.

2.2.8. EPMA analysis

The electron probe microanalysis (EPMA) samples were analyzed by EPMA−1720 Series (Shimadzu corporation) at Kunming university of science and technology center, Yunnan, China, using a 15 kV accelerating voltage and a 20 nA probe current to study the surface variation of the malachite before and after $(NH_4)_3PO_4$ enhancing. The beam diameter was (50 μm), and the counting durations were 15 s on peak and 10 s on the background, respectively. Elements examined include S, P, C, N, Cu, and O.

2.2.9. ToF−SIMS analysis

The chemical composition of malachite surfaces was studied after being treated with $(NH_4)_3PO_4$ and Na_2S using a ToF−SIMS IV (ION−TOF, Munster, Germany). Malachite was cut into symmetrical cubes

(8 mm×8 mm), and sandpaper smoothed the sample. Subsequently, negative spectra were measured with S_2^-, Cu^-, SO_3^-, S^-, and CO_3^-. The images were taken from areas of interest, generally with a (500×500 μm²) of the primary beam's raster.

3. Results and discussion

3.1. Single mineral micro-flotation experiments

Single mineral micro-flotation experiments were carried out to study the effect of $(NH4)_3PO_4$ on the floatability of the malachite. Meanwhile, a xanthate collector 5×10^{-4} mol/dm³ was used at pH 8.7 as shown in Fig. 3. The floatability of the mineral increased as the xanthate concentration increased Fig. 3a. It was observed that the flotation recovery was low when using Na_2S + NaBX. In contrast, the rate increased when $(NH_4)_3PO_4$ was added before the Na_2S treatment, respectively, as seen in Fig. 3b, whether the presence or absence of $(NH_4)_3PO_4$, the malachite recovery was found to increase at first and then decrease as Na_2S concentration increase. From these findings, it was clear that ammonium ions significantly affected the flotation recovery and sulfidation of malachite.

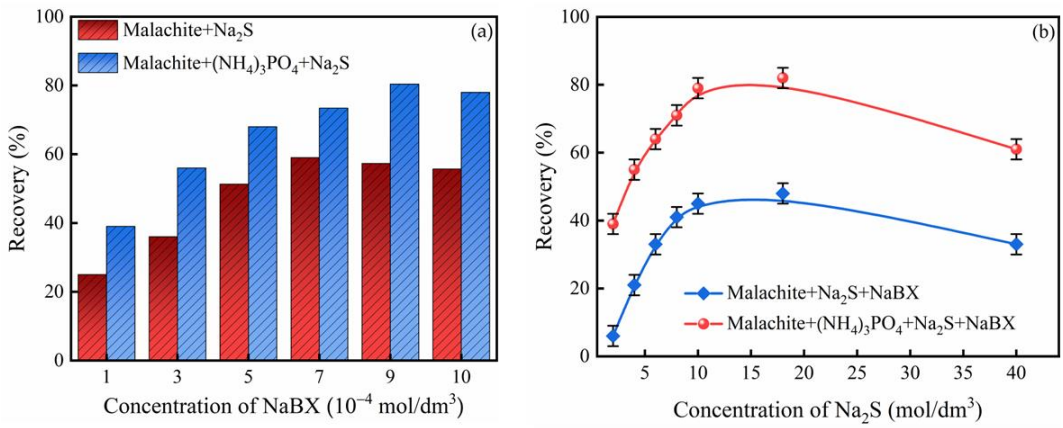

Fig. 3. Flotation recovery of malachite as a function of concentrations (a) NaBX and (b) Na_2S. (2×10^{-3} mol/dm³ Na_2S; 2×10^{-3} mol/dm³ $(NH_4)_3PO_4$ and 5×10^{-4} mol/dm³ NaBX)

3.2. XRD analysis

Fig. 4a illustrates the X−ray diffraction spectra of pure malachite and sulfidation products obtained from malachite treated with 2×10^{-3} mol/dm³ Na_2S and 2×10^{-3} mol/dm³ $(NH_4)_3PO_4$. The results shown in Fig. 4b revealed that covellite (CuS) was the primary mineral species formed on the malachite surface due to the reaction with sulfide ions adsorbed. In contrast, Fig. 4c indicated the increasingly intense peaks growing higher reactions, pointing to the increased crystallinity of the malachite products in the copper-deficient $Cu^{2-x}S$ phases after being treated with $(NH_4)_3PO_4$ (Tezuka et al., 2007).

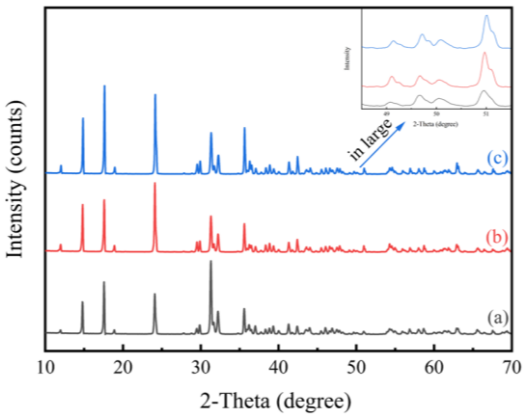

Fig. 4. X−ray diffraction pattern of (a) pure malachite, (b) with Na_2S, and (c) with $(NH_4)_3PO_4$ + Na_2S. Na_2S (2×10^{-3} mol/dm³ Na_2S; 2×10^{-3} mol/dm³ $(NH_4)_3PO_4$ and 5×10^{-4} mol/dm³ NaBX)

3.3. Contact angle measurements

To quantify the correlation between recorded contact angle and water absorption, the angle formed by the solid-liquid interface plays a significant role in engineering fields such as phase separation and other engineering desalination processes like boiling and condensation (Tezuka et al., 2007; Krainer and Hirn, 2021). Fig. 5a showed the contact angle of natural malachite was found to be 69°. The contact angle increased from 69° to 77° after being treated with 2×10^{-3} mol/dm^3 Na_2S, as shown in Fig.5b, demonstrating an increase in the hydrophobicity of the malachite surface. Furthermore, Fig. 5 c showed the contact angles of malachite surfaces after being treated with 2×10^{-3} mol/dm^3 $(NH_4)_3PO_4$ + 2×10^{-3} mol/dm^3 Na_2S was determined to identify the influence of $(NH_4)_3PO_4$ on the malachite floatability during sulfidization at the pH of 8.7.

The contact angle increased from 77° to 88°. The interfacial tension between the malachite surface and liquid was strong after $(NH_4)_3PO_4$ was added before Na_2S, indicating high surface energy and interfacial tension between the two. Moreover, the increasing contact angle of the sulfurized malachite surface might be attributed to the formation of copper sulfide products, thus enhancing the malachite surface hydrophobicity. These phenomena are consistent with previous results of the micro-flotation experiments (Said et al., 2022; Zhang et al., 2022).

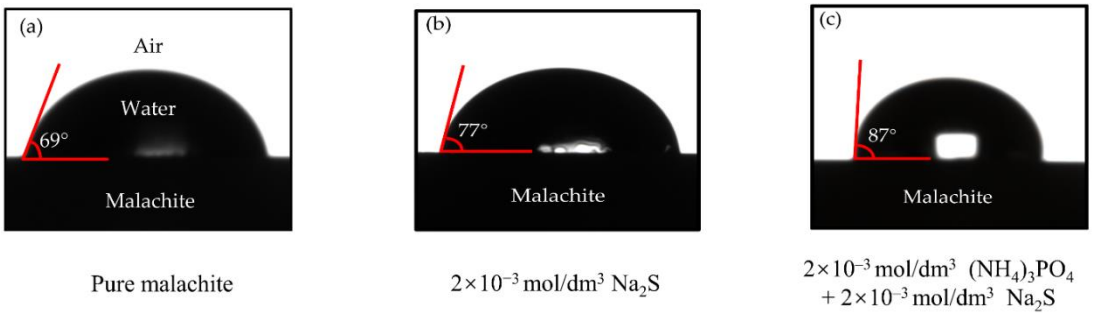

Fig. 5. Contact angles on the malachite surface following pure malachite (a), with Na_2S and with $(NH_4)_3PO_4$ + Na_2S (b)

3.4. Fourier transform infrared (FT−IR) spectroscopy analysis

The FTIR spectra of Na_2S and $(NH_4)_3PO_4$ are shown in Fig. 6. The FTIR spectrum of Na_2S Fig. 6a demonstrated one chemisorption band at 3416 cm^{-1}, which corresponded to the typical O−H group peaks; moreover, the peaks at 2574, 2469 correlated to CO_2 dissolved, and 1637 cm^{-1} was attributed to −C(=S)−N.H. groups, respectively. In addition, Fig. 6b shows that one adsorption peak at 3124 cm^{-1} was visible in the $(NH_4)_3PO_4$ FTIR spectrum, and the adsorption peaks near 2390 and 2211 cm^{-1} were caused by N−N vibrations, which were related to the absorption peaks of N−H groups. The C=O vibration bands were observed near 1716 cm^{-1} (Liu et al., 2018; Yuan et al., 2022).

Fig. 7 shows the malachite after sulfidization with Na_2S and enhanced sulfidization with $(NH_4)_3PO_4$ and Na_2S. In Fig. 7b, the bands detected at 3404 and 3314 cm^{-1} were identified as belonging to O−H stretching vibrations, while the bands located at lower wavelengths of 1804 cm^{-1} were mainly ascribed to out-of-plane stretching vibrations, implying that using only Na_2S to sulfidize the malachite surface is insufficient to form more S ions on the surface, which can improve flotation. Moreover, Fig. 7b revealed that the malachite after $(NH_4)_3PO_4$ treatment and before added Na_2S at pH 9. Meanwhile, the $-NH_2$ group's stretching (from 3404 to 3405 cm^{-1}) and bending (from 1494 to 1507 cm^{-1}) and 1636 cm^{-1} vibration promoted the attachment of the NH_3 ligand to the Cu^{2+} ion (Mahata et al., 2021), respectively, suggesting that $(NH_4)_3PO_4$ may have played a significant part in preparing and enhancing the surface of malachite for a subsequent reaction with Na_2S. Besides, the electron cloud density had shifted from the C−S group to the Cu atom to form Cu−S bonds on the surfaces of the malachite.

In the case compared between Figs. 7a and 7b had longer wavenumbers, it was observed that three new peaks appeared on the surface C−H, C=O, and C=C at 2920, 2850, and 1636 cm^{-1} when the malachite was treated with $(NH_4)_3PO_4$ and Na_2S. In contrast, the peaks were disappeared after treated with only Na_2S. This bond formation suggests that H bonds exist between the interpenetrating NH_4^+ ions and the host $(NH_4)_3PO_4$.

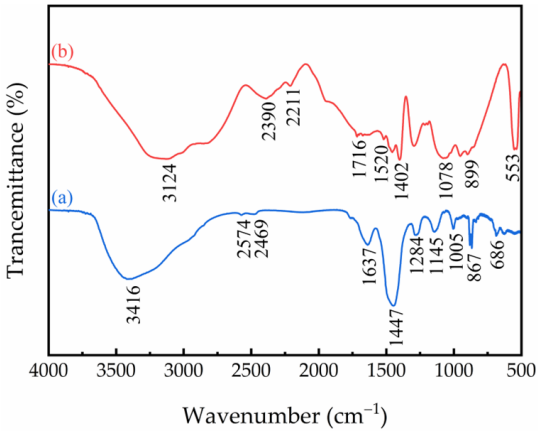

Fig. 6. FTIR spectra of the (a) Na_2S and (b) $(NH_4)_3PO_4$

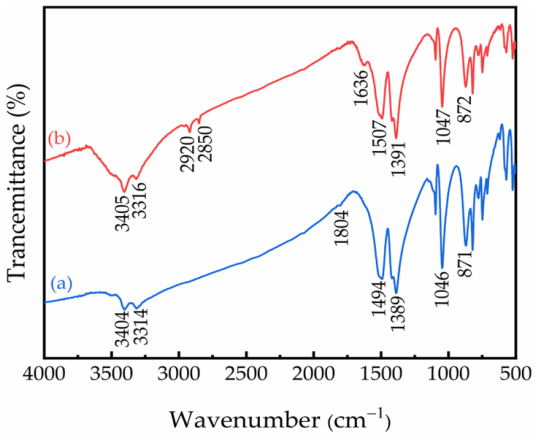

Fig. 7. FTIR spectra of the (a) malachite + Na_2S and (b) malachite + $(NH_4)_3PO_4$ + Na_2S. Na_2S (2×10^{-3} mol/dm^3 Na_2S; 2×10^{-3} mol/dm^3 $(NH_4)_3PO_4$ and 5×10^{-4} mol/dm^3 NaBX)

3.5. Zeta potential measurements

Fig. 8 shows the zeta potentials of malachite samples treated with different reagents to investigate how the $(NH_4)_3PO_4$ addition can affect the adsorption of S ions and xanthate on the malachite surface as a function of pH at the range 5.5-11.5. Malachite's treatment with Na_2S and the isoelectric points (IEPs) are roughly pH 6-7 and pH < 2, and malachite's surface charge changed from positive to negative, suggesting that sulfur ion species were characteristically adsorbed, respectively. These findings are consistent with previous research (Zhang et al., 2022). However, adding $(NH_4)_3PO_4$ prior to Na_2S leads to a negative reduction in zeta potential, implying the increasing sulfur ion species typically adsorbed on the malachite surface, as shown in Fig. 8a. Besides that, Fig. 8b demonstrated malachite–$(NH_4)_3PO_4$–Na_2S−NaBX surface observed a higher number of negative zeta potential, which illustrates that xanthate was adsorbed on the negatively charged malachite surface. Furthermore, in comparison to Fig. 8a, the zeta potential decreased with the increasing pH after adding xanthate collectors. However, this increases the sulfidization of the malachite surface and the xanthate collector's adsorption, attempting to point to the malachite surface's high stability (Singh et al., 2022).

3.6. XPS analysis

Figs. 9a and 9b showed that an XPS analysis was conducted on the malachite sulfurized sample, an enhanced sulfurized sample. The S peak was formed on the malachite surface after it was treated with Na_2S, illustrating that products containing sulfur were produced on the malachite surface. Nevertheless, compared to the Na_2S treatment, the intensity of the peak was more significant when it was treated with $(NH_4)_3PO_4$ + Na_2S, suggesting that more S species were formed on the surface, which indicated that further changes in the chemical environment on the malachite's surface.

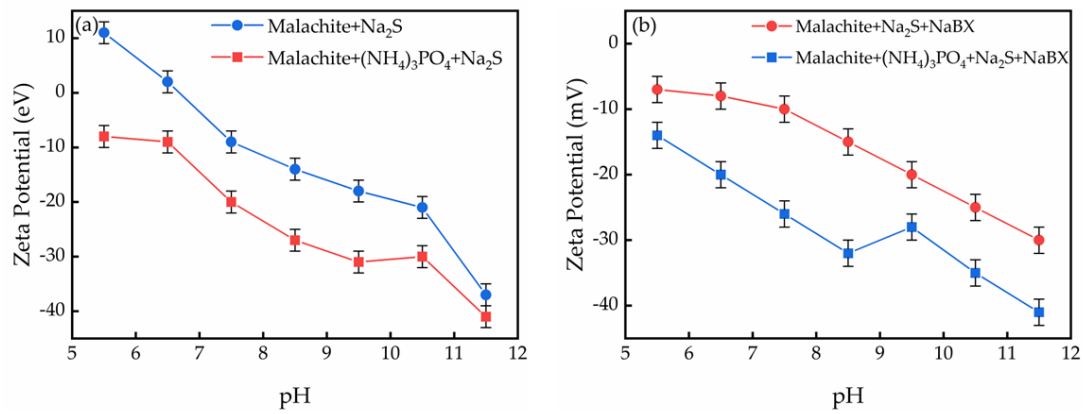

Fig. 8. Zeta potential of malachite as a function of the pH with different flotation reagents: (a) without NaBX; (b) with NaBX. Na_2S (2×10^{-3} mol/dm^3 Na_2S; 2×10^{-3} mol/dm^3 $(NH_4)_3PO_4$ and 5×10^{-4} mol/dm^3 NaBX)

The corresponding contents of the elements C, O, Cu, N, and S on the malachite surface were treated with different chemical reagents as shown in Table 2. When malachite was treated with Na_2S or $(NH_4)_3PO_4$ +Na_2S (predicated on the Cu 2p peak), the S content was increased from 3.16% to 5.24%, and the Cu content also increased from 11.93% to 13.34%. Furthermore, compared to malachite treated with only Na_2S concentration, the content of N in the malachite surface was measured after being treated with $(NH_4)_3PO_4$ and Na_2S, which was found to be 2.06%. Normally, it was not adsorbed to the malachite surface. This can be a result of the effective role that $(NH_4)_3PO_4$ played in the reaction, which made this small amount of adsorbing on the surface. Consequently, it might be concluded that $(NH_4)_3PO_4$ only regulates the sulfurization of malachite and does not contribute to the formation of sulfurized products (Sarojini and Vijayalakshmi., 2022).

The binding energies of the malachite surface treated with 2×10^{-3} mol/dm^3 Na_2S at 932.34 eV are attributed to Cu(I) species. The higher-intensity peak of 934.44 eV is attributed to Cu (II) species shown in Fig. 10a. Whereas the malachite samples after pre-sulfidized with $(NH_4)_3PO_4$ concentration Fig. 10b, the binding energy shifted to 932.53 eV and 934.85 eV, which ascribed to Cu(I) species and Cu (II) species, respectively. The malachite pre-treatment with $(NH_4)_3PO_4$ concentration significantly affected the malachite surface's chemical environment. Nonetheless, the Cu(I) and Cu (II) binding energy have changed in a range of (0.19 eV and 0.41 eV) respectively. This result indicates that copper-sulfide species were significantly formed and adsorbed on the malachite surface, increasing the mineral's hydrophobicity. Furthermore, this results in improved physical characteristics on the mineral surface. The Cu content also increased from 53.68% to 65.39% binding energy in total Cu proportions based on Cu 2p, as displayed in Table 3 (Cai et al., 2022).

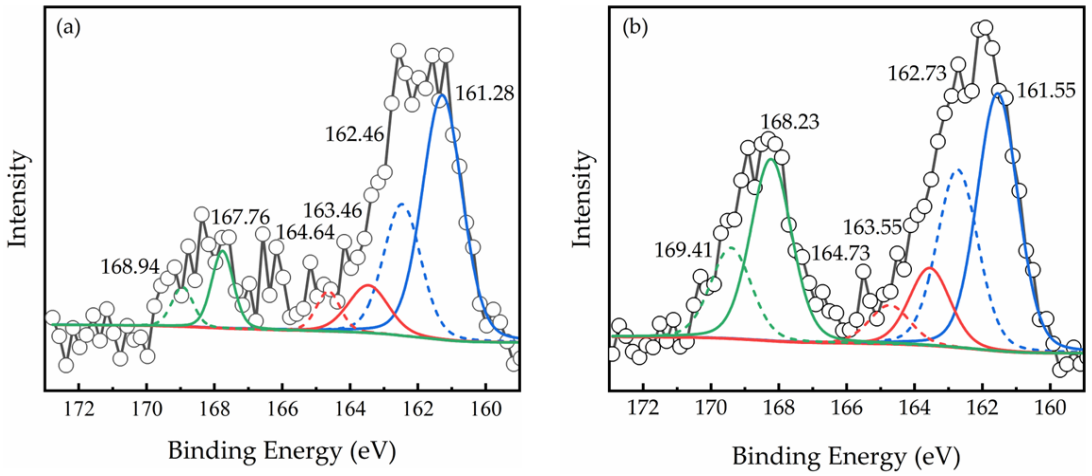

Fig. 9. S 2p XPS spectra of malachite surfaces treated with: (a) 2×10^{-3} mol/dm^3 Na_2S, (b) 2×10^{-3} mol/dm^3 $(NH_4)_3PO_4$ + 2×10^{-3} mol/dm^3 Na_2S

Table 2. Cu 2p quantifications of malachite treated with $Na_2S.9H_2O$, $(NH_4)_3PO_4$ concentrations of: (a) 2×10^{-3} mol/dm^3 $Na_2S.9H_2O$ and (b) 2×10^{-3} mol/dm^3 $(NH_4)_3PO_4$ + 2×10^{-3} mol/dm^3 $Na_2S.9H_2O$

Sample	Atomic concentration (%)				
	Cu 2p	S 2p	O1s	C1s	N1s
a	11.98	3.16	47.00	37.73	0.00
b	13.34	5.24	45.82	33.53	2.06

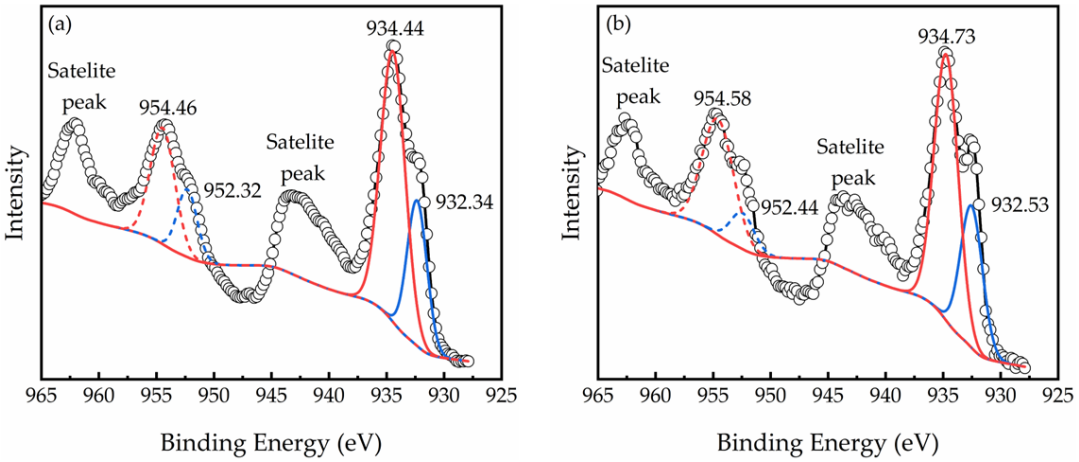

Fig. 10. Cu 2p XPS spectra of malachite surfaces treated with: (a) 2×10^{-3} mol/dm^3 Na_2S, (b) 2×10^{-3} mol/dm^3 $(NH_4)_3PO_4$ + 2×10^{-3} mol/dm^3 Na_2S

Table 3. Binding energy and percentage in total Cu proportions based on Cu 2p XPS spectra obtained from the malachite surface following (a) Na_2S and (b) $(NH_4)_3PO_4$ + Na_2S treatments ($(NH_4)_3PO_4$: 2×10^{-3} mol/dm^3; Na_2S: 2×10^{-3} mol/dm^3)

Sample	Binding energy (eV)		Total Cu (wt.%)	
	Cu (I)	Cu (II)	Cu (I)	Cu (II)
a	932.34	934.44	53.68	46.32
b	932.53	934.73	65.39	34.61

3.7. EPMA analysis

Electron Probe Micro Analyzer (EPMA) mapping was performed on an EPMA-1720 Series (Shimadzu corporation) equipped instrument at Kunming university of science and technology central laboratory to confirm the distribution of the sulfurization on the malachite surface, as shown in Fig. 11. Thus, Figs. 11a and 11b illustrate secondary electron images and WDS elemental mapping of sulfidized and enhanced malachite particles.

The sulfur concentrations were demonstrated in the malachite samples that were sulfidized with 2×10^{-3} mol/dm^3 Na_2S solutions. Moreover, the results for normalized N, O, P, S, and Cu contents (wt.%) were 0.00, 44.811, 0.038, 0.121, and 55.03%, respectively. In addition, as appeared in Fig. 11a3, sulfur was detected inside the malachite particles. Meanwhile, in Fig. 11a2, oxygen was observed localized within the outer surfaces of malachite particles, clearly appearing with a sulfur−containing core and an oxygen-containing shell in Fig. 11b2 (Liu et al., 2020). Whereas more sulfur concentrations were observed when the malachite sample was enhanced sulfidized with 2×10^{-3} mol/dm^3 $(NH_4)_3PO_4$ + 2×10^{-3} mol/dm^3 Na_2S solutions in Fig. 11b3, the findings also revealed that the sulfidization product grew selectively on the slit.

The normalized results of N, O, P, S, and Cu contents (wt.%) were 1.25, 20.657, 0.065, 2.067, and 75.961%, respectively. The EPMA results revealed that the content of N wt.% that was identified on the surface after $(NH_4)_3PO_4$ was added, suggesting that the ammonium ions may have played a significant

role in enhancing sulfidization, resulting in a small amount of N being adsorbed on the malachite surface.

Compared with the malachite −Na_2S, the results of normalized wt.% of Cu and S were increased and changed significantly (20.931, 1.941 wt.%) when treated with both $(NH_4)_3PO_4$ and Na_2S, indicating that the ammonium ions might be were played an essential role in sulfidization of the malachite surface.

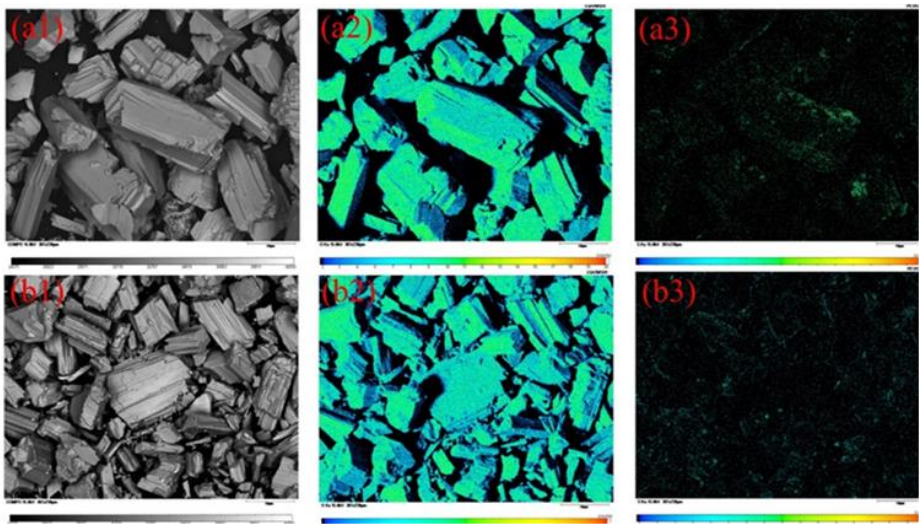

Fig. 11. EPMA surface scan of malachite particles sulfidized with (a) Na_2S and (b) $(NH_4)_3PO_4$ + Na_2S (2×10^{-3} mol/dm^3 Na_2S; 2×10^{-3} mol/dm^3 $(NH_4)_3PO_4$ and 5×10^{-4} mol/dm^3 NaBX). (a1) and (b1) secondary electron images; (a2) and (b2) O elemental mapping; (a3) and (b3) overlays of S elemental mapping

3.8. ToF−SIMS analysis

ToF-SIMS was used to investigate the alterations on the malachite surface as a result of interactions with various reagents (Lai et al., 2020, 2021; Finsgar, 2021). Figs. 12a and 12b show the 2D distributions of S_2^-, Cu^-, SO_3^-, S^-, and CO_3^- ions on malachite after treated with Na_2S and $(NH_4)_3PO_4$ + Na_2S. Respectively, Fig. 12a shows fragment ions on the negative region of S_2^-, Cu^-, SO_3^-, S^-, and CO_3^- were detected on the sulfurized malachite treated with Na_2S; these findings suggest that the element S, which is found in peak fitting results in XPS is reliable. Whereas Fig. 12b illustrates the negative region of S_2^-, Cu^-, SO_3^-, S^-, and CO_3^- ions identified on the surface of malachite after using $(NH_4)_3PO_4$ to enhance the surface before adding Na_2S at different depth ranges, this suggests that the results of malachite's sulfidization are not significantly different throughout a variety of depth ranges. Thus, it was determined that exogenous sulfide ions penetrate distinct interior regions of malachite synchronously (Deng et al., 2019).

Compared with the malachite treated with Na_2S, which observed that the findings in Fig. 12b after $(NH_4)_3PO_4$ exposure before the sulfidization, more S species were produced on the malachite surface. Additionally, a higher percentage of copper oxide species were converted to copper sulfide species, thus which resulted in a rise in the floatability of the malachite (Ibrahim et al., 2022). In addition, after Na_2S treatment, a trace amount of CO_3^- was spread on the malachite surface Fig. 12a. Conversely, slightly increasing CO_3^- ion concentrations were observed after exposure to $(NH_4)_3PO_4$ + Na_2S as seen in Fig. 12b. As seen in Figs. 13a, 13b, and 13c, the pure malachite treated only with water was green, besides malachite treated with Na_2S was dark green, demonstrating that only a slight of copper sulfide species formed on malachite. The malachite color changed to black after being treated with $(NH_4)_3PO_4$ + Na_2S, signifying that the malachite surface was wholly coated with copper sulfide species stable.

4. Conclusions

This work aimed to investigate improving the physical characteristics of the malachite surface employing $(NH_4)_3PO_4$ and Na_2S and the conclusions were as follows:

The results for the micro-flotation experiments indicated that $(NH_4)_3PO_4$ had a better effect on the surface when added before Na_2S, which increased the floatability and significantly improved the malachite's physical characteristics.

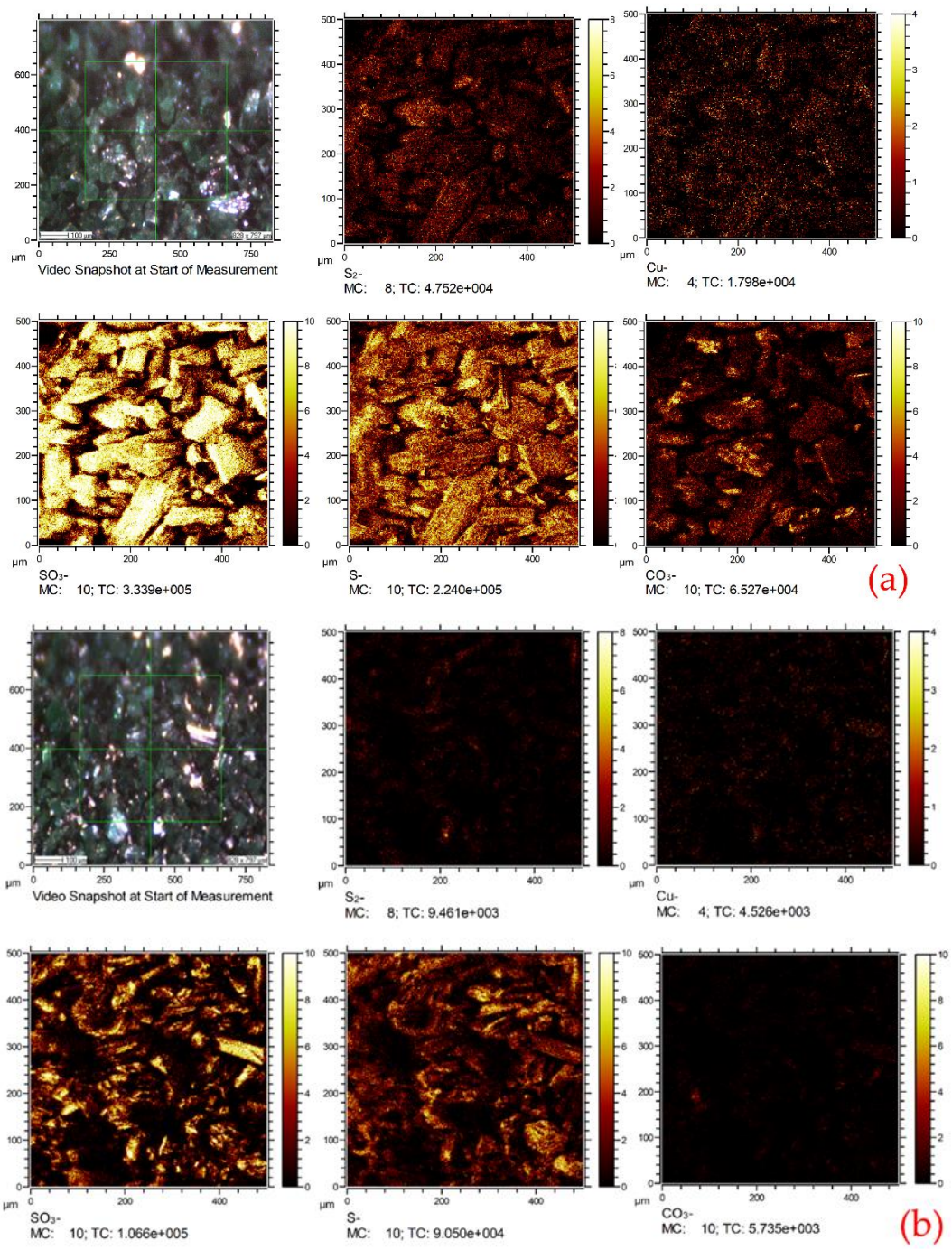

Fig. 12. ToF–SIMS negative ion images of the malachite surface are as follows: (a) treated with Na_2S, and (b) treated with 2×10^{-3} mol/dm^3 $(NH_4)_3PO_4$ + 2×10^{-3} mol/dm^3 Na_2S

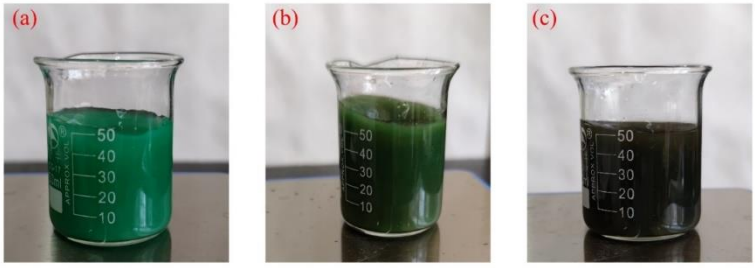

Fig. 13. Malachite treated with (a) water; (b) treated with 2×10^{-3} mol/dm^3 Na_2S and (c) 2×10^{-3} mol/dm^3 $(NH_4)_3PO_4$ + 2×10^{-3} mol/dm^3 Na_2S

The malachite suspension exhibits increased surface stress when the concentration of slurry increases. Meanwhile, malachite particles tended to attach to air bubbles more than other particles due to increased pulp density.

The XPS and EPMA results showed that a small content of N was measured at 2.06% and 1.25%, respectively on the malachite surface. This contributed to a higher content of Cu(I) species and increased sulfide species forming on the mineral surface in the malachite + $(NH_4)_3PO_4$ + Na_2S reaction.

Fourier transform infrared spectroscopy (FTIR) results demonstrated the formation and adsorption of the new distinctive peak of −C(=S)−N.H. groups at 1636 cm^{-1} on the surfaces of malachite.

The malachite contact angle of surface tension and ToF−SIMS analysis revealed that adding ammonium phosphate increased the synthesis of copper sulfide products. Overall depending on the ToF−SIMS analysis showed a significant role played after the $(NH_4)_3PO_4$ was introduced to improve the surface, thereby increasing the ability of malachite floatability as a result of enhancing the physical properties.

Acknowledgments

This research project was supported by the National Natural Science Foundation of China (Grant No. 52074138), Yunnan Major Scientific and Technological Projects (Grant No. 202202AG050015), Basic research project of Yunnan Province (GrantNo.202001AS070030 and 202201AU070099).

References

BELKASSA, K., KHELIFA, M., BATONNEAU-GENER, I., MAROUF-KHELIFA, K., 2021. *Understanding of the mechanism of crystal violet adsorption on modified halloysite: Hydrophobicity, performance, and interaction*. Journal of Hazardous Materials, 415, 125656.

CAI, J., SHEN, P., LIU, D., ZHANG, X., FANG, J., SU, C., YU, X., LI, J., WANG, H., 2021. *Growth of covellite crystal onto azurite surface during sulfurization and its response to flotation behavior*. International Journal of Mining Science and Technology, 31(6), 1003–1012.

CAI, J., S.U., C., YU, X., LIU, R., ZHANG, X., SHEN, P., 2022. *Understanding the mechanism for promoting azurite sulfurization with ammonium sulfate*. Minerals Engineering, 177, 107368.

CECILE, J.L., CRUZ, M. I., BARBERY, G., FRIPIAT, J.J. (1981). *Infrared spectral study of species formed on malachite surface by adsorption from aqueous salicylaldoxime solution*. Journal of Colloid and Interface Science, 80(2).

CHEN, X., PENG, Y., BRADSHAW, D., 2014. *The separation of chalcopyrite and chalcocite from pyrite in cleaner flotation after regrinding*. Minerals Engineering, 58, 64–72.

CHEN, D., LIU, M., HU, B., DONG, Y., XUE, W., HE, P., CHEN, F., ZHU, J., ZHANG, C., 2021. *New insights into the promotion mechanism of $(NH_4)_2SO_4$ in sulfidization flotation: A combined experimental and computational study*. Physicochemical Problems of Mineral Processing, 57(5), 57–70.

DENG, J., LAI, H., WEN, S., LI, S., 2019. *Confirmation of interlayer sulfidization of malachite by TOF-SIMS and principal component analysis*. Minerals, *9*(4), 204.

FENG, Q., ZHAO, W., WEN, S., 2017. *Surface modification of malachite with ethanediamine and its effect on sulfidization flotation*. Applied Surface Science, *436*, 823–831.

FENG, Q., ZHAO, W., WEN, S., 2018. *Ammonia modification for enhancing adsorption of sulfide species onto malachite surfaces and implications for flotation*. Journal of Alloys and Compounds, 744, 301–309.

FINSGAR, M., 2021. *Surface analysis by gas cluster ion beam XPS and ToF-SIMS tandem M.S. of 2-mercaptobenzoxazole corrosion inhibitor for brass*. Corrosion Science. 56-78.

HAN, G., WEN, S., WANG, H., FENG, Q., 2021a. *Sulfidization regulation of cuprite by pre-oxidation using sodium hypochlorite as an oxidant*. International Journal of Mining Science and Technology, 31(6), 1117–1128.

HAN, G., WEN, S., WANG, H., FENG, Q., 2021b. *Surface sulfidization mechanism of cuprite and its response to xanthate adsorption and flotation performance*. Minerals Engineering, 169, 106982.

HE, Z., LIU, G., YANG, X., LIU, W., 2016. *A novel surfactant, N, N -diethyl- N 0 -cyclohexylthiourea: Synthesis, flotation and adsorption on chalcopyrite*. Journal of Industrial and Engineering Chemistry, 37, 107-114.

HU, P., LIANG, L., XIE, G., ZHOU, S., PENG, Y., 2020. *Effect of slurry conditioning on flocculant-aided filtration of coal tailings studied by low-field nuclear magnetic resonance and X-ray*. International Journal of Mining Science and Technology, *30*(6), 859–864.

HUANG, K., CAO, Z., WANG, S., YANG, J., ZHONG, H., 2019. *Flotation performance and adsorption mechanism of styryl phosphonate mono-iso-octyl ester to malachite*. Colloids and Surfaces A, 579, 123698.

IBRAHIM, A. M., JIA, X., SU, C., CAI, J., SHEN, P., LIU, D., 2022. *Effect of ammonium sulfide on sulfidization flotation of malachite*. 1–14. Minerals, *12*(10), 1–14.

KRAINER, S., HIRN, U., 2021. *Effect of liquid absorption and drop size*. Colloids and Surfaces A: Physicochemical and Engineering Aspects, 619, 126503.

LAI, H., LIU, Q., DENG, J., WEN, S., LIU, Z., 2020. *Surface chemistry study of Cu-Pb sulfide ore using ToF-SIMS and multivariate analysis.* Applied Surface Science, 518, 146270.

LAI, H., DENG, J., LIU, Q., WEN, S., SONG, Q., 2021. *Surface chemistry investigation of froth flotation products of lead-zinc sulfide ore using ToF-SIMS and multivariate analysis*. Separation and Purification Technology, 254, 117655.

LEE, J.S., NAGARAJ, D.R., COE, J.E., 1998. *Practical aspects of oxide copper recovery with alkyl hydroxamates*. Minerals Engineering, 11(10), 929–939.

LI, F., ZHOU, X., and LIN, R., 2020. *Flotation performance and adsorption mechanism of novel 1-(2-hydroxyphenyl)hex-2-en-1-one oxime flotation collector to malachite*. Transactions of Nonferrous Metals Society of China, 30(10), 2792–2801.

LIU, S., ZHONG, H., LIU, G., XU, Z., 2018. *Cu(I)/Cu(II) mixed-valence surface complexes of S-[(2-hydroxyamino)-2-oxoethyl]-N,N-dibutyldithiocarbamate: Hydrophobic mechanism to malachite flotation*. Journal of Colloid and Interface Science, 512, 701–712.

LIU, R., LIU, D., LI, J., LI, J., LIU, Z., JIA, X., YANG, S., LI, J., NING, S., 2020. *Sulfidization mechanism in malachite flotation: A heterogeneous solid-liquid reaction that yields CuxSy phases grown on malachite*. Minerals Engineering, 154.

MAHATA, B.K., CHUNG, K., CHANG, S., 2021. *Removal of ammonium nitrogen (NH_4^+-N) by Cu-loaded amino-functionalized adsorbents*. Chemical Engineering Journal, 411, 128589.

SAID, Z., ASLAM, M., WALVEKAR, R., LIU, C., 2022. *Impact of sonication durations on thermophysical properties, contact angle and surface tension of f-MWCNTs nanofluid for heat transfer*. Journal of Molecular Liquids, 358, 119164.

SAROJINI, S. VIJAYALAKSHMI, R.V., 2022. *XPS studies on silver ion conducting solid electrolyte SbI_3-Ag_2MoO_4*. Materials Today: Proceedings.125-143.

SHENG, Q., YIN, W., YANG, B., CAO, S., SUN, H., MA, Y., CHEN, K., 2021. *Improving surface sulfidization of azurite with ammonium bisulfate and its contribution to sulfidization flotation*. Minerals Engineering, 171, 107072.

SHENG, Q., YIN, W., YANG, B., CHEN, K., SUN, H., 2021. *Promotion of oxidation pretreatment on sulfidation of cuprite surface and its contribution to flotation*. Minerals Engineering, 174, 107256.

SINGH, V., KUMAR, A., ALAM, M., KUMAR, A., KUMAR, P., GOYAT, V., 2022. *A study of morphology, U.V. measurements and zeta potential of zinc ferrite and Al_2O_3 nanofluids*. Materials Today: Proceedings, 59, 1034–1039.

TEZUKA, K., SHEETS, W.C., KURIHARA, R., JIN, Y., IMOTO, H., MARKS, T.J., POEPPELMEIER, K.R., 2007. *Synthesis of covellite (CuS) from the elements*. Solid State Sciences, 9, 95–99.

THAKUR, N.V, KARTHA, V.B., KANEKAR, C.R., MARATHE, V.R., 1972. *Infrared spectra of cupferron and some rare earth cupferrates*. Journal of Inorganic and Nuclear Chemistry, 34(9), 2831–2836.

WANG, G., YANG, H., LIU, Y., TONG, L., AUWALU, A., 2020. *Study on the mechanical activation of malachite and the leaching of complex copper ore in the Luanshya mining area, Zambia*. International Journal of Minerals, Metallurgy and Materials, 27(3), 292–300.

WANG, C., SUN, L., WANG, Q., WANG, Y., CAO, Y., WANG, X., CHEN, P., 2022. *Adsorption mechanism and flotation behavior of ammonium salt of N-Nitroso-N-phenylhydroxyamine on malachite mineral*. Applied Surface Science, 583, 152-189.

WU, D., MA, W., MAO, Y., DENG, J., WEN, S., 2017. *Enhanced sulfidation xanthate flotation of malachite using ammonium ions as activator*. Scientific Reports. 1–9.

YOSHIMURA, T., MIYAKE, C., S.I., 1972. *Ultraviolet and infrared spectra of cupferron and neocupferron*. Bulletin of the Chemical Society of Japan, 45(5), 1424-1430.

YUAN, Q., MEI, G., LIU, C., CHENG, Q., YANG, S., 2022. *A novel sulfur-containing ionic liquid collector for the reverse flotation separation of pyrrhotite from magnetite*. Separation and Purification Technology, 122-189.

ZHANG, Q., WEN, S., FENG, Q., WANG, H., 2022. *Enhanced sulfidization of azurite surfaces by ammonium phosphate and its effect on flotation*. International Journal of Minerals, Metallurgy and Materials, 29(6), 1150–1160.